Anal Bioanal Chem (2013) 405:8515–8523
DOI 10.1007/s00216-013-7261-y

RESEARCH PAPER

Total synchronous fluorescence spectroscopic data modeled with first- and second-order algorithms for the determination of doxorubicin in human plasma

Agustina V. Schenone · María J. Culzoni · Andres D. Campiglia · Héctor C. Goicoechea

Received: 17 May 2013 / Revised: 3 July 2013 / Accepted: 15 July 2013 / Published online: 8 August 2013
© Springer-Verlag Berlin Heidelberg 2013

Abstract In this work, we present the development of a method for the determination of doxorubicin in plasma samples in the presence of an unexpected component (riboflavin) by using total synchronous fluorescence spectroscopic data matrices. To the best of our knowledge, this is the first time that the second-order advantage is obtained with this kind of data. Two strategies including unfolding the data and: (a) processing with multivariate curve resolution coupled to alternating least-squares as first-order data or (b) processing with unfolded partial least-squares and exploiting the second-order advantage by the residual bilinearization procedure were considered. The calibration set was built with human plasma samples spiked with doxorubicin, while the validation set was prepared with human plasma samples spiked with both doxorubicin and riboflavin, a drug whose spectrum highly overlaps with the one corresponding to doxorubicin. Both methodologies reached good indicators of accuracy: recoveries of ca. 100±8 % and REP of ca. 5 %; and precision: coefficient of variations between 7 and 9 %.

Keywords Total synchronous fluorescence spectroscopy · MCR-ALS · UPLS/RBL · Doxorubicin

A. V. Schenone · M. J. Culzoni · H. C. Goicoechea (✉)
Laboratorio de Desarrollo Analítico y Quimiometría (LADAQ), Cátedra de Química Analítica I, Facultad de Bioquímica y Ciencias Biológicas, Universidad Nacional del Litoral, Ciudad Universitaria, Santa Fe S3000ZAA, Argentina
e-mail: hgoico@fbcb.unl.edu.ar

A. D. Campiglia
Department of Chemistry, University of Central Florida, Orlando, FL 32816, USA

Introduction

In the last years, chemometrics has gained an important place in analytical chemistry due to its ability to analyze complex multi-component mixtures without resorting to separation procedures. Multivariate calibration methods can be classified similarly to analytical instrumentation, i.e., in zero, first, second, and higher order. In the progression from zero to first- to second-order calibration and beyond, the algorithms become more powerful as the information that they can reliably extract from the data increases [1].

Synchronous fluorescence spectra (SFS) are one kind of first-order data, which are used to overcome complicated multi-component samples with severely overlapping emission and/or excitation spectra. Synchronous spectrometry consists essentially in simultaneously scanning both monochromators, while maintaining a constant wavelength interval ($\Delta\lambda$) between them. The simplification of the spectral profile together with the reduction of band width is its main characteristic [2]. Furthermore, there is a reduction in both Rayleigh and Raman scattering; thus, corrections or preprocessing methods are no longer needed as may happen for excitation-emission spectra [3].

It is important to note that although SFS spectra are narrower and sharper compared to conventional fluorescence spectra, it is not always possible to avoid spectral overlap in certain multi-component mixtures. However, combining SFS spectra with a multivariate method makes the analysis simple and fast without an extraction step [4].

First-order algorithms allow one to identify new samples containing unexpected components, a property known as the first-order advantage [5]. These calibration methods may compensate for potential interferences, usually by their inclusion in the calibration set. On the other hand, second- and higher-order calibration methods can handle the presence of

potential interferences not included in the calibration set, which is the basis of the second-order advantage. This also enables several analytes to be determined simultaneously [5].

Total synchronous fluorescence spectroscopy (TSFS) provides the total synchronous fluorescence characteristics of a multi-fluorophoric sample at various possible wavelength intervals ($\Delta\lambda$). Every TFSF datum consists in a two-way array of dimension excitation wavelength$\times\Delta\lambda$ and can be successfully handled by second-order multivariate calibration algorithms.

In order to apply the proper multivariate algorithm, it is of great importance to know whether the data are trilinear or not because this property is assumed by the underlying models of some of the available algorithms [6]. Second-order data are trilinear when each compound in all experiments treated together can be described by a triad of invariant pure profiles [7], and the spectral shape of a component is not modified by changes in the other two modes (dimensions) [8]. Models with this structure are parallel factor analysis (PARAFAC) [9] and several versions of alternating trilinear decomposition [10–14]. On the other hand, models allowing for deviations of multilinearity in one way or another are multivariate curve resolution coupled to ALS (MCR-ALS) [15], unfolded partial least-squares (U-PLS) [16], multi-way PLS (N-PLS) [17], PARAFAC2 (a variant of PARAFAC that allows profile variations in one of the data dimensions from sample to sample) [18], among others. TSFS behaves in the latter mode, meaning that most of the fluorophores show variation in their spectral shapes along with their spectral intensities as long as $\Delta\lambda$ changes. Each fluorophore in TSFS does not have a single unique SF spectrum due to the fact that the SF spectral shape of a fluorophore varies with the change in offset [19]. Kumar and Mishra were able to simultaneously quantitate five polycyclic aromatic hydrocarbons using TSFS with multivariate methods such as N-PLS, U-PLS, and MCR-ALS, but no second-order advantage was achieved since all the components were added in both calibration and test samples [20]. The same authors have addressed the issue of lack of trilinearity converting the TSFS data to an excitation–emission fluorescence matrix, so that PARAFAC modeling could be applied [21].

The requirement of equal profiles in all dimensions and all samples for a given component is not fulfilled neither in the case of MS/MS data because a given component displays various different profiles in one of the data dimensions. N-PLS with the aid of data preprocessing was found to give good results when this type of non-bilinear data was analyzed. However, all the components were also provided in training and test samples [22].

Doxorubicin (DOX) is an anthracycline antibiotic produced by *Streptomyces peucetius varieta caesius* and is presently used in the treatment of a wide variety of cancers [23, 24]. Numerous HPLC methods have been applied for the determination of DOX and its metabolites in pharmaceutical dosage forms and biological fluids [25–29], as well as HPLC coupled to mass spectrometry [30, 31]. Zagotto et al. described several developments in separation and quantitation of doxorubicin and other anticancer agents in biological fluids, including capillary electrophoresis, UV–visible spectroscopy, and HPLC techniques [32]. Recently, a rapid analysis of doxorubicin and danorubicin was developed by Lu and co-workers using microchip capillary electrophoresis [33].

Direct determination of DOX in human plasma was accomplished based on excitation-emission matrix fluorescence measurements and multiway chemometric PARAFAC and N-PLS [34]. However, the calibration set was built with plasma samples spiked with DOX, and no determinations were done on test samples with unknown constituents.

The objective of this work is to prove whether TSFS combined with multivariate methods such as MCR-ALS and U-PLS coupled to residual bilinearization (RBL) can be used for the quantification of DOX in plasma samples in the presence of overlapping fluorescence due to riboflavin (RF), without any pre-treatment step and calibrating only with DOX. RF is a water-soluble vitamin critical for metabolism and energy production. It presents native fluorescence emission, and it is found in biological fluids, such as plasma. The emission spectrum of RF overlaps with that of DOX, then it was selected as the uncalibrated interference.

One of the most interesting characteristics of this work is the second-order advantage gained for first time in non-bilinear data. This goal has been achieved in two different ways: (a) from first-order responses (the two-way data were unfolded assuming that the unfolded-TSFS data set have a bilinear structure [19]) modeled with MCR-ALS, and (b) from second-order responses modeled by U-PLS/RBL, which has already been proved to achieve the so-called second-order advantage from instrumental data deviating from the trilinearity [16, 35, 36]. Concerning the application of MCR-ALS, it has been demonstrated that the achievement of the second-order advantage, considering and processing first-order multivariate data, is possible, especially when the correlation constraint is used [37–40].

Materials and methods

Chemicals and reagents

Analytical reagent-grade chemicals and ultrapure water, obtained from a Milli-Q water purification system from Millipore (Bedford, MA, USA), were used. Doxorubicin hydrochloride (94.0 %) and riboflavin (96.9 %) were obtained from Richmond Laboratories (Buenos Aires, Argentina). Trichloroacetic acid (TCA) was obtained from Anedra (San Fernando, Argentina) and HPLC grade methanol from Aberkon (Buenos Aires, Argentina).

Stock solution of DOX (455.0 mg L^{-1}) and RF (60.0 mg L^{-1}) were prepared by dissolving the appropriate amount of drug in Milli-Q water and methanol, respectively. Solutions were stored in the dark at 4 °C. Working standards were freshly prepared by diluting stock solutions to desired concentrations with Milli-Q water. Heparinized human plasma samples from untreated healthy volunteers were obtained from Iturraspe Hospital of Santa Fe, Argentina, and stored at −20 °C until the experiments were performed.

Preparation of calibration and validation samples

The calibration set was built by adding pure standard of DOX to plasma obtained from healthy patients due to the presence of interactions between the analyte and the sample background (see below). The set was prepared in two steps: first, five water standards of DOX with the following concentrations: 8.0, 24.1, 40.0, 56.9, and 72.8 μg mL^{-1} were prepared in duplicate. Then, 20.0 μL of the latter solutions was placed into an Eppendorf vial together with 600.0 μL of plasma. After adding 20 μL of TCA 20 % (*w*/*v*) for protein precipitation, each standard sample was vortex mixed for 30 s and ultracentrifuged at 14,000 rpm for 10 min. Then, 500.0 μL of the supernatant was transferred to a quartz cell. The final concentration values of the calibration set were: 0.25, 0.75, 1.25, 1.78, and 2.28 μg mL^{-1}. The protein precipitation step was performed to eliminate a possible matrix effect and to enhance the sensitivity of the method, since plasma proteins provide a significant quenching.

Furthermore, a validation set of nine samples was prepared. First, following a full central composite design of two factors with one center point, with different concentrations of DOX (from 16.0 to 64.0 μg mL^{-1}) and RF (from 2.4 to 9.6 μg mL^{-1}) were prepared in water. Then, the same procedure described for calibration samples preparation was applied. The final concentrations of DOX and RF in the validation set are given in Table 1. These concentrations are within the therapeutic values of the studied drug in human plasma [25].

Instrumentation and software

All spectrofluorimetric measurements were performed using a Perkin-Elmer LS-55 luminescence spectrometer equipped with a xenon discharge lamp, Monk-Gillieson type monochromators, and a gated photomultiplier connected to a PC microcomputer via a RS232C connection. Slits for the excitation and emission monochromators were kept at 10 nm, and the detector voltage was 650 V. TSF spectra were acquired with excitation between 489.5 and 614.5 nm at a resolution of 0.5 nm, with offsets ranged from 30 to 160 nm (in steps of 10 nm) between excitation and emission monochromators. Hence, the size of each data matrix was 251 × 14. In order to analyze DOX, RF, and plasma fluorescence characteristics, excitation–emission spectra were also collected at emission

Table 1 Predictions and statistical analysis of DOX in test samples

Sample	Nominal		Predicted DOX			
	DOX (μg mL^{-1})	RF (μg mL^{-1})	MCR-ALS[a] (μg mL^{-1})	Rec. (%)	U-PLS/RBL[a] (μg mL^{-1})	Rec. (%)
1	0.50	0.19	0.42 (1)	84.0	0.43 (1)	86.0
2	1.78	0.27	1.72 (1)	97.6	1.73 (1)	97.2
3	1.25	0.30	1.28 (1)	102.4	1.28 (1)	102.4
4	1.99	0.19	1.95 (1)	98.0	1.91 (1)	96.0
5	1.25	0.19	1.33 (1)	106.4	1.32 (1)	105.6
6	0.72	0.27	0.76 (1)	105.6	0.73 (1)	101.4
7	1.25	0.075	1.38 (1)	110.4	1.36 (1)	108.8
8	0.72	0.11	0.67 (1)	93.1	0.69 (1)	95.8
9	1.78	0.11	1.77 (1)	99.4	1.80 (1)	101.1
Rec. (%)[a,b]				100 (8)		99 (7)
RMSE (μg mL^{-1})[c]				0.07		0.06
REP (%)[d]				5		5

[a] Between parenthesis the standard deviation

[b] Mean recovery (percentage)

[c] Root mean square error, $\mathrm{RMSE} = \left[\frac{1}{I}\sum_{1}^{I}\left(c_{\mathrm{act}}-c_{\mathrm{pred}}\right)^{2}\right]^{1/2}$, where $I=9$

[d] Relative error of prediction, $\mathrm{REP} = 100 \times \mathrm{RMSE}/\overline{c}$, where $\overline{c}$ is the mean calibration concentration

wavelengths from 500 to 660 nm (every 0.5 nm) with excitation wavelengths from 400 to 480 nm (every 5 nm).

For data processing, all implemented routines were performed using the software MATLAB 7.1 [41]. A useful interface for data input and parameters setting written by Olivieri et al. [42] was employed for U-PLS/RBL implementation. MCR-ALS correlation constrained was implemented using a MATLAB code which is available on internet (http://www.mcrals.info/).

Theory

MCR-ALS

The multivariate calibration algorithm MCR-ALS has been extensively described in the literature [8, 15, 43] so, only a brief description of it is given here. The bilinear decomposition of the augmented matrix **D** is performed according to the expression:

$$\mathbf{D} = \mathbf{C}\mathbf{S}^{\mathrm{T}} + \mathbf{E} \tag{1}$$

in which the rows of **D** contain the unfolded synchronous spectra measured for different samples at several excitation wavelengths, the columns of **C** contain the relative concentrations of the intervening species, the columns of **S** their related unfolded spectra, and **E** is a matrix of residuals not fitted by the model.

Decomposition of **D** is achieved by iterative least-squares minimization of the Frobenius norm of **E**, under suitable constraining conditions during the ALS procedure. MCR-ALS requires initialization with system parameters as close as possible to the final results. In the present work, we employed the SIMPLISMA (simple to use interactive self-modeling mixture analysis) methodology [44] in all cases.

During the iterative recalculations of **C** and $\mathbf{S}^{\mathrm{T}}$, a series of constraints are applied to give physical meaning to the obtained solutions. In this paper, non-negativity of spectra and concentration profiles and correspondence among species in the experiments were used as restrictions. A correlation constraint was also applied during the MCR-ALS analysis, in which the analyte concentrations in the calibration samples at each ALS iteration were forced to be correlated to previously known reference concentration values of the analyte in these samples. More details about the implementation of this constraint in previous works can be found elsewhere [37, 45].

U-PLS/RBL

The essentials of U-PLS/RBL have already been discussed [46]. In the U-PLS method, the original second-order data are unfolded into vectors before PLS is applied. In this algorithm, concentration information is employed in the calibration step, without including data for the unknown sample. The number of latent factors (A) can be selected by techniques such as leave-one-out cross-validation [47].

When unexpected components take place in the test samples, the RBL procedure is then applied to the unfolded test sample data and the outcome scores are free from interferents signal, providing the so-called second-order advantage to the methodology.

Analytical figures of merit

The most important process for comparison of analytical methods is the determination of figures of merit. The estimation of these parameters in multi-way calibration has been subject of several papers in recent literature [48–51]. Sensitivity (SEN), defined as the change in net response for a given change in analyte concentration, can be considered as one of the most relevant figures of merit in the field of analytical chemistry owing to the fact that it is a decisive factor in estimating others, such as limit of detection (LOD), limit of quantitation (LOQ), uncertainty in prediction concentration (SD).

According to Olivieri and coworkers [50], the following expression estimates the SEN when MCR-ALS is applied:

$$\mathrm{SEN}_{\mathrm{MCR}} = m_n \left[J \left(\mathbf{S}^T \mathbf{S} \right)^{-1}_{nn} \right]^{-1/2} \tag{2}$$

in which n is the index for the analyte of interest in a multicomponent mixture, m_n is the slope of the MCR pseudounivariate calibration graph for this analyte, S^T is a matrix containing the profiles for all sample components in the nonaugmented MCR direction, and J is the number of channels in the test sample data matrix in the augmented MCR direction.

In the case of U-PLS/RBL, Allegrini and Olivieri [51] developed a new expression which allows estimating SEN for the multivariate calibration methods based on least-squares regression combined with RBL:

$$\mathrm{SEN}_{JAC} = \left\{ \mathbf{v}^{\mathrm{T}} \left[\mathbf{P}^{\mathrm{T}} (\mathbf{I} - \mathbf{Z}_{\mathrm{int}} \mathbf{Z}_{\mathrm{int}}{}^{+}) \mathbf{P} \right]^{-1} \mathbf{v} \right\}^{-1/2} \tag{3}$$

in which the subscript "*JAC*" stands for the Jacobian approach, **P** is the matrix of calibration loadings, **v** is the vector of PLS regression coefficients in latent variable space, **I** is a unit matrix, and $\mathbf{Z}_{\mathrm{int}}$ contains information regarding the interfering agents.

In the present report, the above presented expressions were used to estimate SEN. LOD, LOQ, and other figures of merit were also analyzed according to the equations in Ref. [50] and [51].

Results and discussion

General considerations

The inspection of the contour plots of the excitation–emission spectra (Fig. 1) recorded from pure DOX in water and RF in water shows that their excitation maxima are at 480 and 445 nm, respectively, and their emission maxima are at 555 m and 520 nm, respectively. Furthermore, this figure displays the spectrum of deproteinized human plasma, showing that there is a substantial overlap among the spectra of all of them. Therefore, the quantitation of DOX in plasma in the presence of RF through a univariate calibration method is difficult. Multivariate methods involving the analysis of more than one variable at a time can be used for the analysis of such samples without any separation.

Figure 2a compares the synchronous fluorescence spectra at $\Delta\lambda$=80 nm of an aqueous solution of pure DOX and the spectral difference between a plasma sample with and without DOX. This offset value was chosen because it corresponds to the difference between emission and excitation maxima (the exact difference is 75 nm, but the experimental measurements were carried out between 30 and 160 nm, each 10 nm). It can be seen that the interaction with the plasma background significantly decreases the fluorescence intensity of the analyte. In order to evaluate if this behavior remained the same in different plasma samples, the slopes of univariate calibration curves (plotting fluorescence intensity at λex=480 nm and λem=555 nm vs. DOX concentration) built with DOX standards prepared in three different plasma samples were statically compared. Since p value for the slopes was 0.913 (p>0.1), there is no statistically significant difference between them at 90 % confidence level. For this reason, the calibration samples were prepared by adding pure DOX standard to plasma.

Figure 2b shows several spectra of pure DOX at different $\Delta\lambda$. As can be seen, the shape of the SF spectra of the fluorophore changes with the change in offset, so TSFS are considered to be non-bilinear data. Therefore, two strategies were implemented to deal with this kind of data: unfolding and modeling with MCR-ALS achieving the second-order advantage with first order data as was done in a reduced number of papers [37–40], and modeling with PLS exploiting the second-order advantage implementing the RBL procedure [16].

MCR-ALS

Previously to data analysis, each matrix (size, 251×14) was unfolded into a vector of size 1×3,514. For quantitation, data matrices corresponding to test samples have to be simultaneously analyzed with those of the standards. Then, all the matrices were disposed in a column-wise augmented matrix (size, 19×3,514).

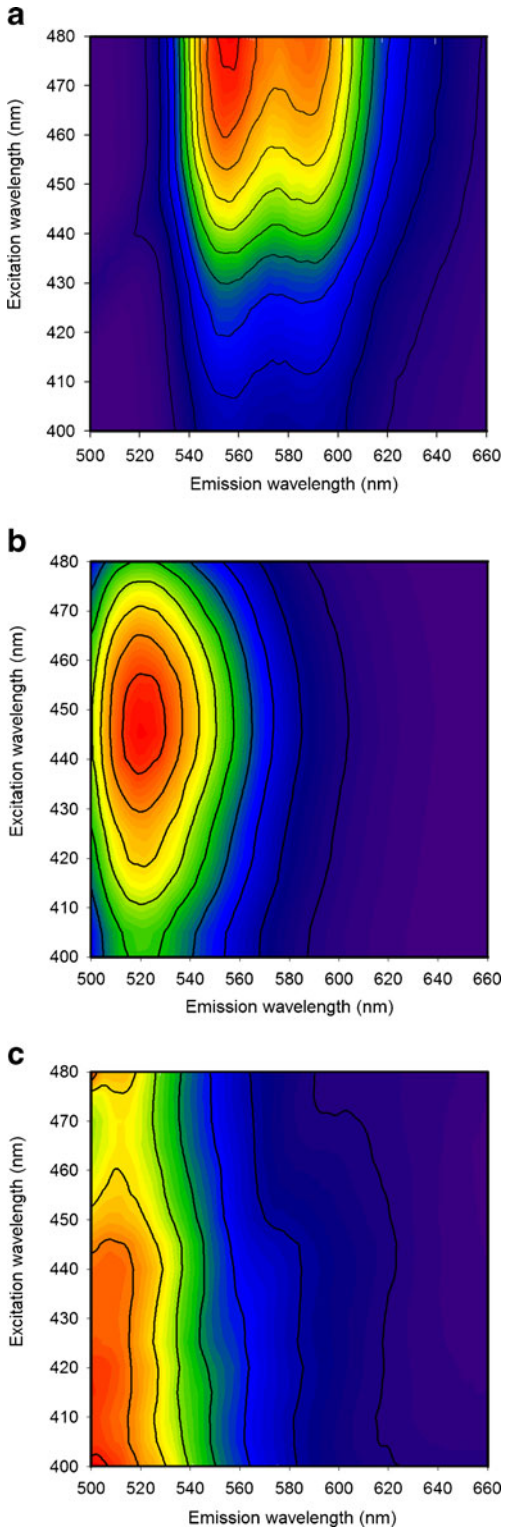

Fig. 1 Excitation–emission contour plot for pure DOX in water (**a**), RF in water (**b**), and deproteinized human plasma (**c**)

The estimation of the number of pure components in the system was assessed by the application of singular value decomposition to the augmented data matrix, suggesting that there were three significant factors. The initial estimations for

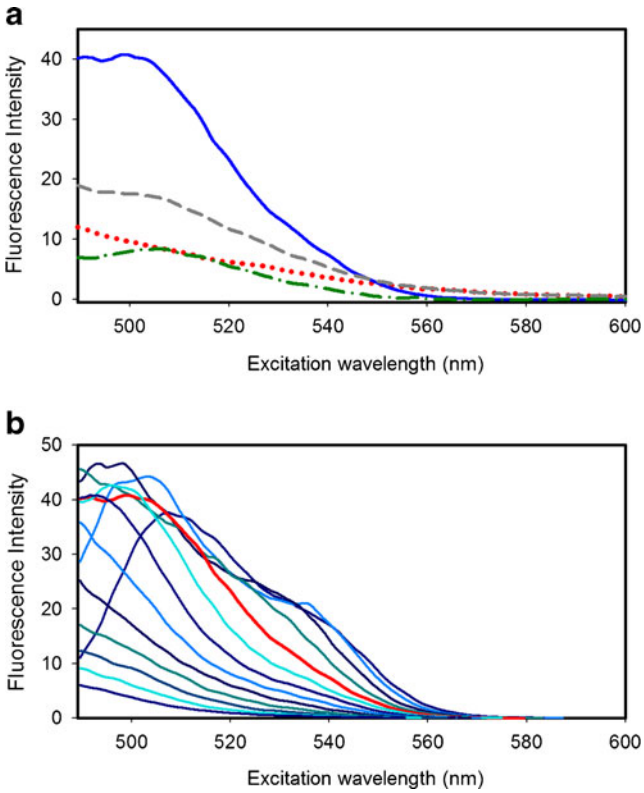

Fig. 2 **a** Synchronous fluorescence spectra of pure DOX 1.25 μg mL^{-1} (*solid line*), plasma containing DOX 1.25 μg mL^{-1} (*dashed line*), spectral difference between a plasma containing DOX 1.25 μg mL^{-1}, and a blank plasma (*dashed dotted line*) and blank plasma sample (*dotted line*), all at $\Delta\lambda$=80 nm. **b** Synchronous fluorescence spectra of pure DOX 1.25 μg mL^{-1} at several $\Delta\lambda$ (from 30 to 160 nm, each 10 nm). In *red*, spectra at $\Delta\lambda$=80 nm

MCR-ALS were obtained by the selection of the purest variables based on SIMPLISMA [44].

The implementation of adequate constraints during optimization makes the output less subjected to ambiguities. In the present work, the constraints listed in "MCR-ALS" section were applied. Special attention should be paid to the correlation constraint, which forces the standard concentration to be correlated to previously known values during the ALS optimization. A local linear model between the ALS estimated values and the nominal concentrations is built by least-squares linear regression. Concentration values are then updated according to the predicted values using the estimated parameters of the local model. In the present work, a matrix with the same size of **C** (19×3) was provided as initial input, containing in the first ten lines the nominal concentration for DOX in calibration samples, as well as the information that plasma, but no interferent was present in these samples. The next nine lines indicated the presence of the three compounds in test samples as unrestricted values (NaN).

Convergence was achieved in 38 consecutive iterative cycles when the selected MCR convergence criterion was reached (relative change in fit for successive iterations=0.1 %). The value of lack of fit was 2.43 % and the explained variance, 99.94 %. Figure 3 shows the recovered spectra in the matrix $\mathbf{S}^T$ after the ALS optimization. Although the overlapping is significant, the spectra corresponding to DOX and the interferences were properly retrieved by MCR-ALS. In the inset of Fig. 3, the spectra obtained for the three components and the normalized spectrum of pure DOX are shown, all of them at $\Delta\lambda$=80 nm, which is the optimum offset value for the analyte. As can be seen, the pure and the recovered DOX spectra satisfactorily match (with a r^2 ca. 1), indicating that the extracted profile corresponds to the analyte of interest.

Quantitation was performed by regressing the scores values obtained in the matrix **C** for each calibration sample against the known concentration values. Figure 4 shows the pseudo-univariate graph, as well as the scores of the test samples, illustrating how analyte scores vary in calibration (circles) and test (crosses) samples, whereas plasma scores (triangles down) remain almost constant, as expected. In the case of RF, there is

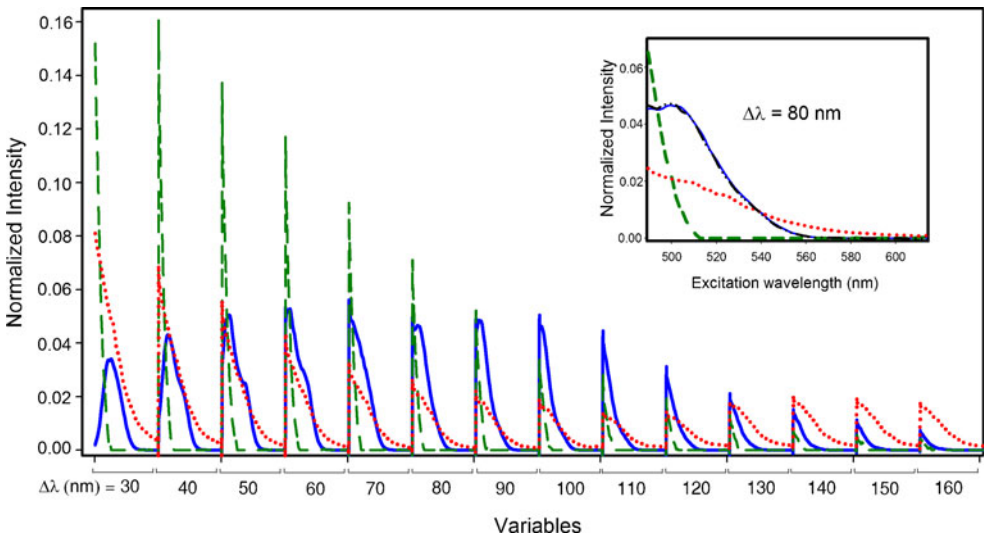

Fig. 3 Recovered spectra in the matrix $\mathbf{S}^T$ after MCR-ALS analysis of the augmented data matrix which contains the validation and calibration samples. The *solid line* corresponds to DOX, the *dashed line* to the interferent RF, and the *dotted line* to plasma background. In the *inset*, the spectra for these three components (DOX: *solid line*, RF: *dashed line*, plasma: *dotted line*) and the normalized spectrum of pure DOX (*dashed-dotted line*) are shown at $\Delta\lambda$=80 nm

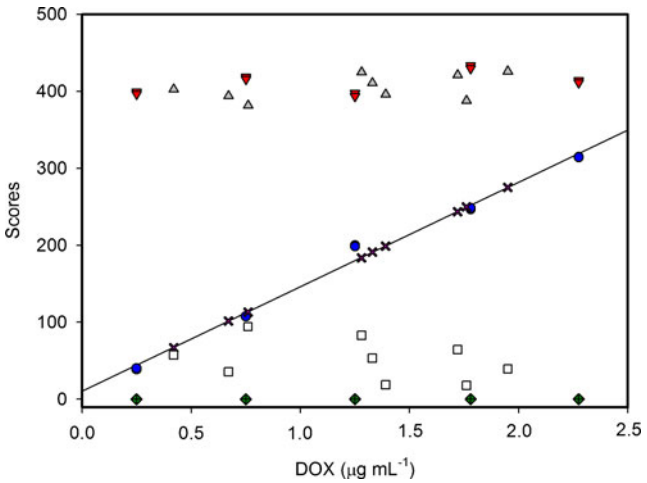

Fig. 4 Score values of DOX (*circles*), RF (*diamonds*), and plasma (*triangles down*) in calibration samples and DOX (*crosses*), RF (*squares*), and plasma in validation (*triangles up*) and calibration (*triangles down*) samples obtained after MCR-ALS optimization

no contribution in calibration samples (diamonds; this fact is expected owing to this was imposed with a constraint), but its presence is noticeable in the validation samples (squares).

Table 1 displays the results obtained for the analysis of the validation mixtures, showing an excellent agreement between nominal and predicted values: the RMSE is 0.07 μg mL^{-1}, implying a REP value of 5 %. Moreover, the precision of the method was evaluated by the analysis of five replicates of test sample number 5 (see Table 1), by the same analyst, under the same conditions, on three different days. The obtained coefficient of variations (CV%) were all below 15 % (see Table 2). ANOVA test was applied to analyze if the variances among the 3 days were comparable. It could be concluded that there is not statistically significant difference among them (p=0.524). These parameters, together with the mean recovery (100±8 %), indicate that the proposed method is a feasible methodology for achieving the second-order advantage in cases of unfolded non-trilinear TSFS data.

U-PLS/RBL

The first phase in data processing is the estimation of the number of responsive components. In the case of U-PLS/RBL, the number of latent variables A is assessed by leave-one-out cross-validation, according to the Haaland and Thomas criterion [47]. In the presently studied case, Fig. 5 shows how the predicted error sum of squares ([PRESS=$\sum(c_{act}-c_{pred})^2$]) varies as the number of latent variables is increased when the calibration set is employed, showing that A=2 is the optimum value, corresponding to the presence of DOX and plasma in the calibration samples.

The RBL method is usually implemented to filter the test sample data from the contribution of unexpected components

Table 2 Figures of merit for the determination of DOX by modeling TSFS data with MCR-ALS and U-PLS/RBL

		MCR-ALS	U-PLS/RBL
SEN (AFU mL μg^{-1})		23	44
γ (mL μg^{-1})[a]		192	370
γ^{-1} (μg mL^{-1})		0.005	0.003
LOD (μg mL^{-1})[b]		0.02	0.01
LOQ (μg mL^{-1})[c]		0.06	0.03
CV (%)[d]	Day 1	8	7
	Day 2	9	7
	Day 3	8	8
ANOVA[e]		F=0.69 (p=0.524)	F=0.51 (p=0.611)

AFU arbitrary fluorescence units

[a] Analytical sensitivity

[b] LOD, limit of detection calculated according to Ref [50] for MCR-ALS and Ref [51] for U-PLS/RBL, considering 95 % of probability

[c] LOQ, limit of quantification calculated as LOD×(10/3.3)

[d] CV, coefficient of variation calculated from validation sample number 5 from Table 1 (n=5) during three consecutive days

[e] Critical $F_{(3-1);(15-3);0.05}$ value equal to 3.89

(N_{unx}). In order to assess this number, the analysis of the residuals s_u obtained with the RBL procedure was done. Figure 5 clearly indicates that the size of residuals stabilizes at N_{unx}=1, owing to the presence of RF in the test samples.

Using two principal components for modeling the calibration data and a single unexpected component for RBL, the U-PLS/RBL methodology was applied to the test samples. The prediction and statistical results for the determination of DOX

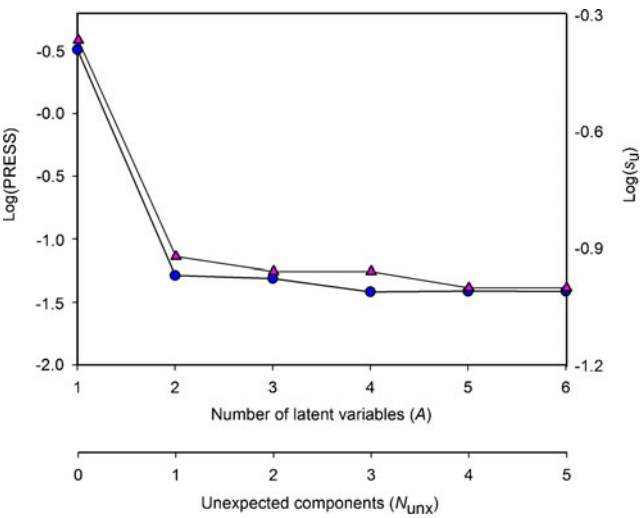

Fig. 5 Logarithm of the leave-one-out cross-validation PRESS [log(PRESS)] as a function of the number of U-PLS latent variables A, constructed using calibration data (*circles*), and logarithm of the U-PLS prediction residuals [log(s_u)] as a function of the number of unexpected components (N_{unx}) (*triangles*)

in these samples using U-PLS/RBL are shown in Table 1, being satisfactory as indicated by the values of mean recovery (99±7 %), RMSE (0.06 μg mL^{-1}), and REP (5 %). In order to assess the precision, the CV% was analyzed. For this purpose, triplicate determinations were carried out on test sample number 5 (see Table 1) on three different days. The CV% values obtained are shown in Table 2. The ANOVA test showed that the variances were comparable for the 3 days ($p>0.05$). As well as MCR-ALS, the lack of trilinearity in TSFS data could be conveniently processed and modelled by using U-PLS/RBL, with the achievement of the second-order advantage.

Analytical figures of merit

With the aim of comparing the performance of various methods, figures of merit such as limit of detection, sensitivity, and analytical sensitivity among others are employed regularly. Table 2 shows the analytical figures of merit obtained when applying the MCR-ALS algorithm according to Ref. [50]. This table also displays the figures of merit corresponding to the U-PLS/RBL application, computed as described in Ref. [51] (see "Analytical figures of merit" section). As can be seen, the sensitivity for U-PLS/RBL is almost twice this value for MCR-ALS. This fact can be due that the second-order structure is maintained when modeling with the former algorithm. In addition, the way in which this analytical figure of merit is computed is totally different. The same is appreciated for the analytical sensitivity, γ, which may be more useful for method comparison, since fluorescence intensity units are arbitrary. It allows one to compare analytical methods regardless of the specific technique, equipment, and scale employed, and its inverse establishes the minimum concentration difference (γ^{-1}) which is statistically discernible by the method. In the present case, γ^{-1} is 0.005 and 0.003 μg mL^{-1} for MCR-ALS and U-PLS/RBL, respectively.

Other important figures of merit are the limit of detection (LOD) and the limit of quantification (LOQ). The detecting capabilities calculated as indicated in Ref. [50] and [51] are also presented in Table 2. There is an improvement in the resulting LOD and LOQ for U-PLS/RBL in comparison with the values obtained for MCR-ALS. This is expected since these terms are affected by the sensitivity parameter.

It is important to remark that the RBL procedure obtains an approximation of the real TSFS corresponding to the interference because it is considered to be bilinear data. Nevertheless, this approximation is enough to reach an acceptable error (REP% ca. 5 %) which is similar to that obtained by modeling the data with a first-order algorithm, a fact that was performed by unfolding the data instead of using them with the second-order structure. Although better figures of merit are achieved when U-PLS/RBL is applied, both algorithms constitute a good alternative for the resolution of plasma samples in the determination of DOX when non-trilinear data are analyzed.

Conclusions

In this work, we demonstrate the possibility of modeling non-bilinear data obtained by TSFS attaining the second-order advantage for the quantitation of DOX in plasma samples in presence of an unexpected component (RF). Two strategies were considered, which include unfolding the data and: (a) processing with MCR-ALS as first-order data, or (b) processing with PLS and exploiting the second-order advantage by the RBL procedure. Both methodologies reach to REP of ca. 5 %, a value that could be considered as acceptable for biological samples. Nevertheless, more efforts should be put in order to develop an algorithm able to model the data maintaining its second-order structure. Research is being carried out in our laboratory in this context.

Acknowledgments The authors are grateful to Universidad Nacional del Litoral (Projects CAI+D Nº 11–11 and 11–7), to CONICET (Consejo Nacional de Investigaciones Científicas y Técnicas, Project PIP 455), and to ANPCyT (Agencia Nacional de Promoción Científica y Tecnológica, Project PICT 2011–0005) for financial support. A.V.S. thanks CONICET for her fellowship.

References

1. Escandar GM, Faber NM, Goicoechea HC, Muñoz de la Peña A, Olivieri AC, Poppi RJ (2007) TrAC Trends Anal Chem 26:752–765
2. Lloyd JBF (1971) Nat Phys Sci 231:64–65
3. Wehry EL (1990) In: Guilbault GG (ed) Practical fluorescence. Marcel Dekker, New York
4. Patra D, Mishra AK (2002) TrAC Trends Anal Chem 21:787–798
5. Booksh KS, Kowalski BR (1994) Anal Chem 66:782A–791A
6. Olivieri AC, Escandar GM, Muñoz de la Peña A (2011) TrAC Trends Anal Chem 30:607–617
7. De Juan A, Tauler R (2003) Anal Chim Acta 500:195–210
8. De Juan A, Tauler R (2001) J Chemom 15:749–772
9. Bro R (1997) Chemom Intell Lab Syst 38:149–171
10. Wu HL, Shibukawa M, Oguma K (1998) J Chemom 12:1–26
11. Chen ZP, Wu HL, Jiang JH, Li Y, Yu RQ (2000) Chemom Intell Lab Syst 52:75–86
12. Xia AL, Wu HL, Fang DM, Ding YJ, Hu LQ, Yu RQ (2005) J Chemom 19:65–76
13. Sanchez E, Kowalski BR (1986) Anal Chem 58:496–499
14. Sanchez E, Kowalski BR (1990) J Chemom 1:29–45
15. Tauler R (1995) Chemom Intell Lab Syst 30:133–146
16. Wold S, Geladi P, Esbensen K, Öhman J (1987) J Chemom 1:41–56
17. Bro R (1996) J Chemom 10:47–61
18. Kiers HAL, Ten Berge JMF, Bro R (1999) J Chemom 13:275–294
19. Kumar K, Mishra AK (2012) Chemom Intell Lab Syst 116:78–86
20. Kumar K, Mishra AK (2011) Anal Methods 3:2616–2624
21. Kumar K, Mishra AK (2012) Anal Chim Acta 755:37–45
22. Zampronio CG, Gurden SP, Moraes LAB, Eberlin MN, Smilde AK, Poppi RJ (2002) Analyst 127:1054–1060
23. Benjamin RS, Riggs CE Jr, Bachur NR (1973) Clin Pharmacol Ther 14:592–600
24. Speth PA, van Hoesel QG, Haanen C (1988) Clin Pharmacokinet 15:15–31
25. Andersen A, Warren DJ, Slordal L (1993) Ther Drug Monit 15:455–461

26. Gotlieb WH, Bruchim I, Ben-Baruch G, Davidson B, Zeltser A, Andersen A, Olsen H (2007) EJSO 33:213–215
27. Chen CL, Thoen KK, Uckun FM (2001) J Chromatogr B Biomed Appl 764:81–119
28. Loadman PM, Calabrese CR (2001) J Chromatogr B Biomed Appl 764:193–206
29. Fahmy OT, Korany MA, Maher HM (2004) J Pharm Biomed Anal 34:1099–1107
30. DiFrancesco R, Griggs JJ, Donnelly J, DiCenzo R (2007) J Chromatogr B 852:545–553
31. Lachâtre F, Marquet P, Ragot S, Gaulier JM, Cardot P, Dupuy JL (2000) J Chromatogr B 738:281–291
32. Zagotto G, Gatto B, Moro S, Sissi C, Palumbo M (2001) J Chromatogr B Biomed Appl 764:161–171
33. Lu H, Yuan G, He Q, Chen H (2009) Microchem J 92:170–173
34. Trevisan MG, Poppi RJ (2003) Anal Chim Acta 493:69–81
35. Culzoni MJ, Goicoechea HC, Pagani AP, Cabezón MA, Olivieri AC (2006) Analyst 131:718–732
36. Goicoechea HC, Olivieri AC (2005) Appl Spectrosc 59:926–933
37. Azzouz T, Tauler R (2008) Talanta 74:1201–1210
38. Goicoechea HC, Olivieri AC, Tauler R (2010) Analyst 135:636–642
39. Llamas NE, Garrido M, Di Nezio MS, Fernández Band BS (2009) Anal Chim Acta 655:38–42
40. Mamián-López MB, Poppi RJ (2013) Anal Chim Acta 760: 53–59
41. MATLAB 7.1. (2005) The MathWorks Inc., Natick: Massachussets, USA
42. Olivieri AC, Wu HL, Yu EQ (2009) Chemom Intell Lab Syst 96:246–251
43. Saurina J, Leal C, Compañó R, Granados M, Prat MD, Tauler R (2001) Anal Chim Acta 432:241–251
44. Windig W, Guilment J (1991) Anal Chem 63:1425–1432
45. Antunes MC, Simao JEJ, Duarte AC, Tauler R (2002) Analyst 127:809–817
46. Olivieri AC (2005) J Chemom 19:615–624
47. Haaland DM, Thomas EV (1988) Anal Chem 60:1193–1202
48. Olivieri AC, Faber NKM, Ferré J, Boqué R, Kalivas JH, Mark H (2006) Pure Appl Chem 78:633–661
49. Olivieri AC, Faber NKM (2012) Anal Chem 84:186–193
50. Bauza MC, Ibañez GA, Tauler R, Olivieri AC (2012) Anal Chem 84:8697–8706
51. Allegrini F, Olivieri AC (2012) Anal Chem 84:10823–10830